ACADEMIC PRESS

Available online at www.sciencedirect.com

SCIENCE DIRECT®

Journal of Computational Physics 185 (2003) 512–531

JOURNAL OF COMPUTATIONAL PHYSICS

www.elsevier.com/locate/jcp

Instability of the time splitting scheme for the one-dimensional and relativistic Vlasov–Maxwell system

F. Huot [a], A. Ghizzo [a], P. Bertrand [a,*], E. Sonnendrücker [b], O. Coulaud [c]

[a] *Laboratoire de physique des milieux ionisés, UMR 7040, BP 239 54506 Vandoeuvre les Nancy, Cedex, France*
[b] *Institut Elie Cartan de Nancy, Université Henri Poincaré I, BP 239 54506 Vandoeuvre les Nancy, Cedex, France*
[c] *INRIA Projet Scalaplix, LaBRI Domaine universitaire 351, 33000 Talence, France*

Received 23 July 2001; received in revised form 5 December 2002; accepted 11 December 2002

Abstract

The Time Splitting Scheme (TSS) has been examined within the context of the one-dimensional (1D) relativistic Vlasov–Maxwell model. In the strongly relativistic regime of the laser–plasma interaction, the TSS cannot be applied to solve the Vlasov equation. We propose a new semi-Lagrangian scheme based on a full 2D advection and study its advantages over the classical Splitting procedure. Details of the underlying integration of the Vlasov equation appear to be important in achieving accurate plasma simulations. Examples are given which are related to the relativistic modulational instability and the self-induced transparency of an ultra-intense electromagnetic pulse in the relativistic regime.

Keywords: Time Splitting Scheme; Vlasov–Maxwell model; Semi-Lagrangian scheme; Laser–plasma interaction; Self-induced transparency

1. Introduction

The numerical integration of the Vlasov–Maxwell system plays an important role in plasma physics, since a knowledge of its nonlinear evolution is indispensable in the understanding of plasmas. Robust numerical methods [1–4], for simulating the temporal evolution of the particle distribution function have been developed. Most of them involve the "Time Splitting Scheme" or TSS of the Vlasov equation. In that scheme the initial Vlasov equation is splitted into two partial derivative equations, one in x, t, the other in v, t. Considering the dimensionless form of the 1D Vlasov–Poisson equations

$$\frac{\partial f}{\partial t} + v\frac{\partial f}{\partial x} + E(x,t)\frac{\partial f}{\partial v} = 0, \tag{1}$$

* Corresponding author.
E-mail address: alain.ghizzo@lpmi.uhp-nancy.fr (P. Bertrand).

0021-9991/03/$ - see front matter
doi:10.1016/S0021-9991(02)00079-7

$$\frac{\partial E}{\partial x} = \int_{-\infty}^{+\infty} f \, \mathrm{d}v - 1, \tag{2}$$

where the symbols have their conventional meaning, the method introduced by Cheng and Knorr [1] consisted in splitting up the free-streaming term and the acceleration term in (1), solving first the free-streaming term

$$\frac{\partial f}{\partial t} + v\frac{\partial f}{\partial x} = 0 \tag{3}$$

and then solving the acceleration term

$$\frac{\partial f}{\partial t} + E(x,t)\frac{\partial f}{\partial v} = 0. \tag{4}$$

The integration of Eqs. (3) and (4) was reduced to the following shifting sequence of the distribution function

$$f^*(x,v) = f^n(x - v\Delta t/2, v), \tag{5}$$

$$f^{**}(x,v) = f^*(x, v - E(x)\Delta t), \tag{6}$$

$$f^{n+1}(x,v) = f^{**}(x - v\Delta t/2, v), \tag{7}$$

where f^n denotes the value of the distribution function at time $t_n = n\Delta t$. The electric field E used in Eq. (6) for the shift of f was calculated from f^* given in Eq. (5). Fourier interpolation or spline interpolation were used to perform the resulting shifts (5)–(7), and the scheme was demonstrated to be very accurate and efficient and correct up to the second-order in Δt.

Although this method uses an Eulerian grid, the shifts along x and v are nothing but Lagrangian advections since the method is equivalent to solving the characteristics of the Vlasov equation making the full scheme a semi-Lagrangian one.

In the simple case considered above, the advection term v (respectively $E(x,t)$) does not depend on the variable along which the shifts are performed x (respectively v), and the solutions (5)–(7) are straightforward. This method proved to work very well in this electrostatic case and also in the relativistic and electromagnetic case where the laser intensity is not too high ($a \ll 1$) (see [6,7,10,11]). The advantage is that the scheme can use larger time steps than explicit Eulerian ones and is noiseless in comparison to particles models (as Particles-In-Cell codes), but the price to pay is to reconstruct a regular grid using interpolation. This method is known to be second-order accurate in time-step (see [2,7]).

However this scheme could not be applied as easily to more complicated Vlasov problem, for instance the drift kinetic Vlasov equation or the relativistic Vlasov equation. In that case we have to consider a problem like

$$\frac{\partial f}{\partial t} + v(x,t)\frac{\partial f}{\partial x} = 0, \tag{8}$$

where the advection term depends on the variable to be advected. In a recent paper [5], we have shown how to solve this problem by introducing the backward characteristic scheme, where (5) (or (7)) is replaced by

$$f^*(x, v, t_n + \Delta t) = f(x - \alpha, v, t_n), \tag{9}$$

where $x - \alpha$ is the starting point of the characteristic ending at x and can be obtained to the second-order accuracy by solving the implicit equation

$$\alpha = \Delta t v\big(x - \alpha/2, t_{n+1/2}\big). \tag{10}$$

In the simple case where the advection field v is a constant with respect to the variable to be advected, as in the 1D Vlasov–Poisson case, the solution of (10) is straightforward and we recover (5)–(7), providing the time splitting holds. For more complex Vlasov models we have shown in [5] how to solve the implicit equation (10). This semi-Lagrangian method or backward characteristic method has been already investigated by the fluid dynamics community and especially in weather and climate simulation (see [12]). The scheme is second-order accurate in time-step (see by example [12–14]) and a mathematical analysis has been performed by Bermejo [13] which has interpreted this method as a finite-element Particles-In-Cell (PIC) method and proves its convergence. But it was also clearly noticed that the time splitting could not be as easily applied as in the electrostatic case. It is the goal of this paper to revisit this point.

The paper is organized as follows. The TSS problem is presented in Section 2. In Section 3 we give the 1D plasma model describing the laser–plasma interaction in the relativistic regime and the governing equations are derived. Issues related to TSS and the generalized 2D advection are then addressed in this section. Numerical comparisons have been carried out in this Section 4. The case of periodic boundary conditions and of the relativistic modulational instability for an underdense plasma is presented in this section. A more complex situation relevant to a causal (open) plasma is then presented in the case of the study of the self-induced transparency of an electromagnetic pulse in an overdense plasma. Conclusion and future work are offered in Section 5.

2. The time splitting problem

Consider the Vlasov equation in the following form

$$\frac{\partial f}{\partial t} + \mathbf{U}(\mathbf{X}, \mathbf{t}) \cdot \nabla_X f = 0, \tag{11}$$

where $\mathbf{X}$ stands for the phase space coordinates and $\mathbf{U}$ is a divergence-free vector field having up to six components in the full 3D case. For example, in the case of the 3D electrostatic Vlasov equation, we have $\mathbf{X} = (x, y, z, v_x, v_y, v_z)$ and $\mathbf{U} = (v_x, v_y, v_z, E_x, E_y, E_z)$, all the components of the electric field depending on x, y, z and t.

For an advection field $\mathbf{U}$ which is divergence free as it happens for the Vlasov equation, Eq. (11) can also be written in conservative form

$$\frac{\partial f}{\partial t} + \mathrm{div}_X(\mathbf{U}(\mathbf{X}, t) f) = 0. \tag{12}$$

Splitting the components of $\mathbf{X}$ into two sets $\mathbf{X}_1$ and $\mathbf{X}_2$, Eq. (12) can then be written in the form

$$\frac{\partial f}{\partial t} + \mathrm{div}_{X_1}(\mathbf{U}_1(\mathbf{X}_1, \mathbf{X}_2, t) f) + \mathrm{div}_{X_2}(\mathbf{U}_2(\mathbf{X}_1, \mathbf{X}_2, t) f) = 0. \tag{13}$$

Moreover, it is well known (see for instance [14]) that solving separately

$$\frac{\partial f}{\partial t} + \mathrm{div}_{X_1}(\mathbf{U}_1(\mathbf{X}_1, \mathbf{X}_2, t) f) = 0, \tag{14}$$

$$\frac{\partial f}{\partial t} + \mathrm{div}_{X_2}(\mathbf{U}_2(\mathbf{X}_1, \mathbf{X}_2, t) f) = 0 \tag{15}$$

keeps the second-order accuracy for the whole Eq. (13) by alternating the solves.

It is now important to point out that the semi-Lagrangian scheme does not solve Vlasov's equation in the conservative form, but in the advective form to make full use of the backward characteristic method. Therefore if (and only if) both conditions hold

$$\mathrm{div}_{X_1}\mathbf{U}_1(\mathbf{X}_1,\mathbf{X}_2,t)=0, \tag{16}$$

$$\mathrm{div}_{X_2}\mathbf{U}_2(\mathbf{X}_1,\mathbf{X}_2,t)=0. \tag{17}$$

Eqs. (14) and (15) can be put in the advective form

$$\frac{\partial f}{\partial t}+\mathbf{U}_1\cdot\nabla_{X_1}f=0, \tag{18}$$

$$\frac{\partial f}{\partial t}+\mathbf{U}_2\cdot\nabla_{X_2}f=0, \tag{19}$$

allowing to keep the second-order accuracy for the whole Eq. (11) by alternating the solves. This is the basis of the time splitting scheme providing the conditions (16) and (17) are fulfilled. This is obviously the case for the 1D electrostatic Vlasov equation (1).

On the contrary, if Eqs. (16) and (17) are not true, then splitting Eq. (11) is equivalent to solve advective equations with a source term

$$\frac{\partial f}{\partial t}+\mathbf{U}_1\cdot\nabla_{X_1}f=-f\,\mathrm{div}_{X_1}(\mathbf{U}_1), \tag{20}$$

$$\frac{\partial f}{\partial t}+\mathbf{U}_2\cdot\nabla_{X_2}f=-f\,\mathrm{div}_{X_2}(\mathbf{U}_2). \tag{21}$$

Although from the divergence-free property of the full advection field $\mathbf{U}$, we have

$$\mathrm{div}_{X_1}(\mathbf{U}_1)=-\mathrm{div}_{X_2}(\mathbf{U}_2) \tag{22}$$

the source term in (20) or (21) do not cancel exactly since in a time splitting scheme (20) and (21) are not solved at the same time.

Therefore, if conditions (16) and (17) are not true, solving (18) and (19) will introduce a cumulative systematic error at each time step, resulting in poor density conservation irrespective of the numerical procedure for solving the time splitted equations. We have demonstrated that a necessary condition for the time splitting to preserve the conservative character of the Vlasov equation is that the advection fields $\mathbf{U}_1$ and $\mathbf{U}_2$ are both divergence free.

3. Case of the 1D relativistic Vlasov equation

To show how an inadequate use of the TSS may affect the nature of the exact solution of the Vlasov equation, we are presenting two examples related to the study of parametric instabilities induced by an intense pump electromagnetic wave in the relativistic regime. Attention in this section is confined to a model which describes purely electronic parametric instabilities. When electrons quiver at relativistic velocities, laser light is subject to new regimes of purely electronic parametric instabilities not evident at lower intensities. Their understanding is basic to the success of many new applications arising in high-field science. These include, among others, the fast ignition concept, or plasma based electron accelerator schemes.

3.1. Plasma model

To describe the behavior of an electromagnetic wave propagating in a relativistic electron gas in a fixed neutralizing ion background we need to solve the relativistic Vlasov equation. Even for the plasma plane wave propagating, let us say, along the x-direction, we have to solve a Vlasov equation for a 4D distribution function $F = F(x, p_x, p_y, p_z, t)$

$$\frac{\partial F}{\partial t} + \frac{p_x}{m\gamma}\frac{\partial F}{\partial x} + e\left(\mathbf{E} + \frac{\mathbf{p}\times\mathbf{B}}{m\gamma}\right)\frac{\partial F}{\partial \mathbf{p}} = 0 \tag{23}$$

with

$$\gamma^2 = 1 + \frac{p_x^2 + p_y^2 + p_z^2}{m^2c^2}. \tag{24}$$

Furthermore it is easy to reduce this 4D Vlasov equation to a 2D Vlasov equation in the following way. Let us consider the Hamiltonian of a particle in the electromagnetic field $(\mathbf{E}, \mathbf{B})$, in the relativistic regime, for a 1D spatial system (x) (i.e., for the plane wave propagation)

$$H = mc^2\left(1 + \frac{(\mathbf{P}_c - e\mathbf{A})^2}{m^2c^2}\right)^{1/2} + e\phi(x,t), \tag{25}$$

where ϕ is the electrostatic potential, $\mathbf{A}$ the vector potential, and $\mathbf{P}_c$ the canonical momentum connected to the particle momentum $\mathbf{p}$ by

$$\mathbf{P}_c = \mathbf{p} + e\mathbf{A}. \tag{26}$$

Choosing the Coulomb gauge (div$\mathbf{A} = 0$) we have $\mathbf{A} = \mathbf{A}_\perp(x,t)$. Let us write the Hamilton equation, where $\mathbf{q} = (x, y, z)$,

$$\frac{\mathrm{d}\mathbf{P}_c}{\mathrm{d}t} = -\frac{\partial H}{\partial \mathbf{q}} \tag{27}$$

along the longitudinal direction (which is also the direction of propagation of the electromagnetic wave)

$$\frac{\mathrm{d}P_{cx}}{\mathrm{d}t} = -\frac{\partial H}{\partial x} \tag{28}$$

and in the transverse direction

$$\frac{\mathrm{d}\mathbf{P}_{c\perp}}{\mathrm{d}t} = -\nabla_\perp H = 0. \tag{29}$$

This last equation means $\mathbf{P}_{c\perp} = \text{const}$. Furthermore, without loss of generality, consider a plasma initially prepared so that we can choose this constant equal to zero. In other words, it means that all electrons at given (x,t) have the same perpendicular momentum components $\mathbf{p}_\perp = -e\mathbf{A}_\perp(x,t)$ and the 4D distribution function $F(x, p_x, \mathbf{p}_\perp, t)$ can be reduced to a 2D distribution function $f(x, p_x, t)$ accounting for the longitudinal electron motion (see for example [9]). The Hamiltonian given by Eq. (25) becomes then

$$H = mc^2\left[1 + \frac{p_x^2}{m^2c^2} + \frac{e^2\mathbf{A}_\perp^2(x,t)}{m^2c^2}\right]^{1/2} + e\phi(x,t) \tag{30}$$

and the corresponding Vlasov equation for the 2D distribution function $f(x, p_x, t)$ simply writes

$$\frac{\mathrm{d}f}{\mathrm{d}t} = \frac{\partial f}{\partial t} + \frac{\partial H}{\partial p_x}\frac{\partial f}{\partial x} - \frac{\partial H}{\partial x}\frac{\partial f}{\partial p_x} = 0. \tag{31}$$

Using Eq. (30) the derivation of the reduced Vlasov equation is straightforward and leads to the following expression

$$\frac{\partial f}{\partial t} + \frac{p_x}{m\gamma_1}\frac{\partial f}{\partial x} + \left(eE_x - \frac{mc^2}{2\gamma_1}\frac{\partial(a^2)}{\partial x}\right)\frac{\partial f}{\partial p_x} = 0, \tag{32}$$

where the normalized potential vector amplitude was given by

$$a^2 = \frac{e^2\mathbf{A}_\perp^2(x,t)}{m^2c^2}. \tag{33}$$

From Eq. (30) and using Eq. (33), the Lorentz factor used in Eq. (32) is

$$\gamma_1 = \left(1 + \frac{p_x^2}{m^2c^2} + a^2(x,t)\right)^{1/2}. \tag{34}$$

Finally, we have to add the Maxwell equations. Our 1D propagation model allows to separate the electric field into two parts

$$\mathbf{E} = E_x\mathbf{e}_x + \mathbf{E}_\perp, \tag{35}$$

where $E_x = -\partial\phi/\partial x$ is a pure electrostatic field, which obeys Poisson's equation and

$$\mathbf{E}_\perp = -\frac{\partial\mathbf{A}_\perp}{\partial t} \tag{36}$$

is a pure electromagnetic field. The transverse electromagnetic fields E_y, B_z and E_z, B_y obey Maxwell's equations, which can be written in the following form (introducing new fields $E^\pm = E_y \pm cB_z$ and $F^\pm = E_z \pm cB_y$)

$$\frac{\partial E^\pm}{\partial t} \pm c\frac{\partial E^\pm}{\partial x} = -\frac{J_y}{\varepsilon_0}, \tag{37}$$

$$\frac{\partial F^\pm}{\partial t} \mp c\frac{\partial F^\pm}{\partial x} = -\frac{J_z}{\varepsilon_0}. \tag{38}$$

These equations are integrated along their vacuum characteristics $x \pm ct = \text{const}$. The transverse current density is then given by

$$\mathbf{J}_\perp(x,t) = \frac{e\mathbf{P}_\perp(x,t)}{m}\int\frac{f}{\gamma_1}\,\mathrm{d}p_x, \tag{39}$$

where the transverse momentum vector $\mathbf{P}_\perp$ is given by $\mathbf{P}_\perp = -e\mathbf{A}_\perp$ according to Eq. (26), where $\mathbf{P}_{c\perp} = 0$.

3.2. Splitting the Vlasov equation

Coming back to the Vlasov equation (32), we have with the notation introduced in Section 2

$$\mathbf{U} = (U_1, U_2) = \left(\frac{p_x}{m\gamma_1}, eE_x - \frac{mc^2}{2\gamma_1}\frac{\partial(a^2)}{\partial x}\right), \tag{40}$$

$$\mathbf{X} = (x, p_x).$$

We have obviously

$$\mathrm{div}_X(\mathbf{U}) = 0 \tag{41}$$

since

$$\frac{\partial}{\partial x}\left(\frac{p_x}{m\gamma_1}\right) + \frac{\partial}{\partial p_x}\left(eE_x - \frac{mc^2}{2\gamma_1}\frac{\partial(a^2)}{\partial x}\right) = 0,$$

which means that $\mathbf{U}$ is divergence free, and furthermore that Vlasov equation (32) is indeed conservative. Unfortunately the presence of the Lorentz γ_1 factor given by (34) couples the variables x and p_x and prevents the splitted fields $\mathbf{U}_1$ and $\mathbf{U}_2$ to be divergence free, since obviously

$$\mathrm{div}_{X_1}\mathbf{U}_1 = \frac{\partial}{\partial x}\left(\frac{p_x}{m\gamma_1}\right) = -\frac{p_x}{2m\gamma_1^3}\frac{\partial}{\partial x}(a^2) \neq 0, \tag{42}$$

$$\mathrm{div}_{X_2}\mathbf{U}_2 = \frac{\partial}{\partial p_x}\left(eE_x - \frac{mc^2}{2\gamma_1}\frac{\partial(a^2)}{\partial x}\right) = -\mathrm{div}_{X_1}\mathbf{U}_1 \neq 0 \tag{43}$$

while, in the nonrelativistic case $\gamma_1 = 1$ and the divergence conditions hold for $\mathbf{U}_1$ and $\mathbf{U}_2$. Thus, it is clear that the time splitting should not be used in the relativistic case since, *from a mathematical point of view*, the necessary conditions given by Eqs. (16) and (17) do not hold. The Vlasov equation (32) is then one example for which the use of the time splitting is not possible when high intensity laser intensities are considered (for $a \gtrsim 1$): since $\gamma_1(x, p_x, t)$ couples the phase space variables, each splitted advection equation does not exactly conserve the density while the global Vlasov equation does.

To check this idea we have written two different codes: one using the time splitting of the Vlasov equation (32) and one based on the direct integration of Eq. (32) using the full 2D advection scheme.

3.3. A Vlasov code using the time spitting

First the TSS was used for solving Eq. (32) according to the following three-step procedure.

Step (A1). Solve the free streaming term over $\Delta t/2$ i.e.

$$\frac{\partial f}{\partial t} + \frac{p_x}{m\gamma_1}\frac{\partial f}{\partial x} = 0 \tag{44}$$

leading to the solution

$$f^*(x, p_x) = f^n(x - \alpha, p_x), \tag{45}$$

where α is given solving the implicit equation

$$\alpha = \frac{\Delta t}{2} U_1\left(x - \alpha/2, p_x, t_{n+1/4}\right) \tag{46}$$

using the numerical procedure described in [5].

Step (A2). Integrate the acceleration equation for a whole time step Δt :

$$\frac{\partial f}{\partial t} + e\left(E_x - \frac{mc^2}{2\gamma_1}\frac{\partial(a^2)}{\partial x}\right)\frac{\partial f}{\partial p_x} = 0. \tag{47}$$

We obtain then the procedure

$$f^{**}(x,p_x) = f^{*}(x,p_x-\beta), \tag{48}$$

where β is solution of

$$\beta = \Delta t U_2\big(x,p_x-\beta/2,t_{n+1/2}\big), \tag{49}$$

where U_1, U_2 are defined by (40).

Step (A3). Repeat step (A1) from $t_{n+1/2}$ to obtain f^{n+1} using:

$$f^{n+1} = f^{**}(x-\alpha,p_x). \tag{50}$$

The step A2 requires the knowledge of the fields at time $t_{n+1/2}$: the longitudinal electric field E_x not being affected by the shift A2 can be computed by solving Poisson's equation

$$\frac{\partial E_x}{\partial x} = \frac{e}{\varepsilon_0}(n_{\mathrm{e}} - n_{\mathrm{i}}) \tag{51}$$

with $n_{\mathrm{e}} = \int f \,\mathrm{d}p_x$ at the end of step A1, $n_{\mathrm{i}} = n_0$ being the ion density and n_0 the mean electron density. But the necessary knowledge of the electromagnetic fields $E^{\pm}$ and $F^{\pm}$, at time $t_{n+1/2}$ suggests solving Maxwell's equations (37) and (38) alternately with the Vlasov equation between $t_{n-1/2}$ and $t_{n+1/2}$ in a leapfrog scheme, in such a way that the contribution of the source term in Eqs. (37) and (38) are centered in time. For example, for Eq. (37) we have

$$E^{\pm\ n+1/2}(x \pm c\Delta t) = E^{\pm\ n-1/2}(x) - \Delta t J_y^n(x \pm c\Delta t/2)/\varepsilon_0, \tag{52}$$

$$J_y^n(x \pm c\Delta t/2) = \frac{J_y^n(x \pm \Delta x) + J_y^n(x)}{2}. \tag{53}$$

Hence, we may integrate exactly along the vacuum characteristics ($x \pm ct = \text{const}$) using grid spacing $\Delta x = c\Delta t$. Finally Eq. (36) is solved between t_n and t_{n+1} using the time centered scheme

$$\mathbf{A}_\perp^{n+1}(x) = \mathbf{A}_\perp^{n}(x) - \Delta t \mathbf{E}_\perp^{n+1/2}(x), \tag{54}$$

which allows to use relation

$$\mathbf{A}_\perp^{n+1/2}(x) = [\mathbf{A}_\perp^{n+1}(x) + \mathbf{A}_\perp^{n}(x)]/2$$

to compute the Lorentz factor γ_1 at time $t_{n+1/2}$.

Consequently, *from a numerical point of view*, the different advections together with Maxwell solution are carefully taken into account through a second-order scheme. But *from a mathematical point of view,* the necessary conditions (16) and (17) are not fulfilled. Thus, we consider now a 2D semi-Lagrangian advective code which does not need the recourse to time splitting.

3.4. Backward semi-Lagrangian Vlasov code using 2D advection

In the case where the time splitting cannot be applied, the only possibility is to integrate the Vlasov equation (32) using full 2D advection. The 2D advection is also of second-order accuracy in time step and allows a direct integration without splitting the Vlasov equation.

Then, given the value of the function f at the mesh points at any given time step (by f^n), we obtain the new value at mesh points using that

$$f^{n+1}(\mathbf{X}) = f^{n}(\mathbf{X} - \boldsymbol{\alpha}), \tag{55}$$

where $\boldsymbol{\alpha}$ is now a 2D vector and is computed using

$$\boldsymbol{\alpha} = \Delta t \mathbf{U}\left(\mathbf{X} - \boldsymbol{\alpha}/2, t_{n+1/2}\right) \tag{56}$$

which can be solved iteratively for the unknown vector $\boldsymbol{\alpha}$. f^{n+1} is then interpolated using a tensor product of cubic B-splines. Again the procedure (55) requires the knowledge of the fields at time $t_{n+1/2}$. Since the distribution function is determined at time t_n, t_{n+1} and so on we may again use previous numerical solver to compute the electromagnetic fields $E^{\pm}$ and $F^{\pm}$ and the corresponding potential vector $\mathbf{A}_{\perp}$. From the above analysis we see that solving Poisson equation to determine the longitudinal electric field E_x at time $t_{n+1/2}$ requires the data of $f^{n+1/2}$, which is unknown here. To avoid this difficulty we have replaced the Poisson equation by the Ampere equation

$$\frac{\partial E_x}{\partial t} = -\frac{J_x}{\varepsilon_0} = -\frac{e}{\varepsilon_0}\int \frac{p_x}{m\gamma_1} f \, \mathrm{d}p_x, \tag{57}$$

which becomes

$$E_x^{n+1/2}(x) = E_x^{n-1/2}(x) - \Delta t J_x^n(x)/\varepsilon_0. \tag{58}$$

At each time step a pseudo electric field $E_x'^{\,n+1/2} = (E_x'^{\,n+1} + E_x'^{\,n})/2$ is computed using Poisson's equation at time t_n and t_{n+1} and the resulting field has been found in well agreement with the solution directly obtained by the Ampere equation.

4. Comparisons between both Vlasov codes

Both Vlasov integration schemes have been implemented on a vectorial NEC-SX5 computer in a monoprocessor and full optimized version. Using open boundary conditions and a phase space grid of $N_x N_{p_x}$ of 4097×513 grid points or 2.103.761 "particles", the first version of the Vlasov code including TSS required a CPU time of 152 s for 500 time steps, i.e., 0.144 μs per particle and per time step in the case of an optimized version of the code of 2.22 Gflops. The backward semi-Lagrangian method, using a tensor product of B-splines requires a CPU time of order of 177 s for the same phase space sampling and the same number of time steps, i.e., 0.168 μs per particle and per time step, the code being a high degree of vectorization of 2.02 Gflops. The numerical effort to "push" a "particle" in both methods is then very similar.

4.1. Numerical comparison in the case of periodic boundary conditions

First the method is tested by computed the vortices induced by the relativistic modulational instability generated by an ultra-intense pump wave in a periodic box. In our example, the pump electromagnetic wave is assumed to be circularly polarized with a dispersion relation given by $\omega_0^2 = \omega_p^2/\gamma_0 + k_0^2 c^2$, (ω_0, k_0) being, respectively, the pump frequency and wave number of the electromagnetic wave, and γ_0 being given by $\gamma_0^2 = 1 + p_{\mathrm{osc}}^2/m^2c^2 = 1 + a_0^2$.

A large amplitude right ($\varepsilon = +1$) circularly polarized electromagnetic wave is initialized in a simulation box with a quiver momentum $a_0 = p_{\mathrm{osc}}/mc = 0.75$ and we have chosen

$$E_y(x, t=0) = E_0 \cos k_0 x; \quad E_z(x, t=0) = \varepsilon E_0 \sin k_0 x. \tag{59}$$

For the magnetic field components we have taken:

$$B_y(x, t=0) = -\varepsilon k_0 E_0 \sin k_0 x/\omega_0; \quad B_z(x, t=0) = -k_0 E_0 \cos k_0 x/\omega_0. \tag{60}$$

The corresponding values of the transverse momentum are then given by

$$P_y(x,t=0) = -eE_0 \sin k_0 x/\omega_0; \quad P_z(x,t=0) = e\varepsilon E_0 \cos k_0 x/\omega_0. \tag{61}$$

The pump wave frequency is $\omega_0 \simeq 1.341\omega_p$ corresponding to a wave number $k_0 c/\omega_p = 2\Delta k c/\omega_p = 1$; $\Delta k = 2\pi/L_x$ being the fundamental mode of the plasma corresponding to a ratio of the plasma density to the critical density of $n_0/n_{crit} \simeq 0.55$. Fig. 1 shows the mean density $\int n_e(x,t)\,dx - 1$, normalized to the ion density as a function of time $t\omega_p$ in (a) and the corresponding time evolution of the total energy in (b). The full line is obtained using the TSS method and 1D advection and the dotted line corresponds to the full 2D integration of the system. The 2D integration was carried out with a time step of $\Delta t\omega_p = 0.02$ and a phase space sampling $N_x N_{p_x} = 256 \times 256$ (with a mass conservation at the end of the simulation, i.e., $t\omega_p = 120$, close to $\Delta n/n_0 = 0.0009$), while the simulation using TSS required a higher sampling $N_x N_{p_x} = 512^2$ to achieve numerical stability. It is clear that the use of the TSS in that case leads to bad conservation of the Vlasov invariant. As shown in Fig. 1, accurate numerical integration can be achieved only using the full 2D advection scheme.

A large amplitude plane light (ω_0, k_0) couples any plasma fluctuation at (ω, k) to a hierarchy of sidebands at $(\omega + l\omega_0, k + lk_0)$. At low intensities, Stimulated Raman Scattering, the decay into a resonant electron plasma wave and Stokes $(l = -1)$ and possibly anti-Stokes $(l = 1)$ electromagnetic sidebands, is the dominant decay mechanism. At extreme intensities, the Fourier modes become strongly coupled with

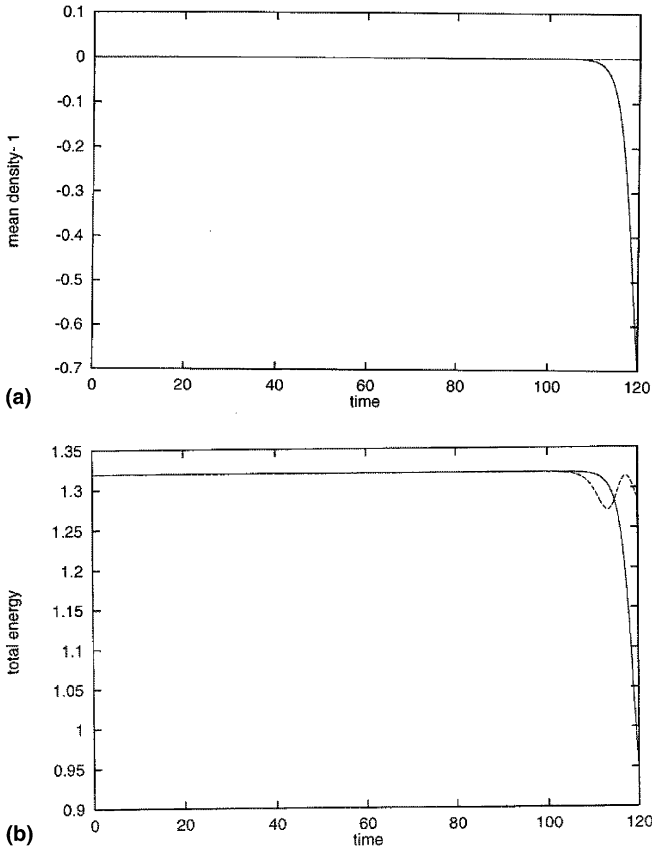

Fig. 1. Numerical comparison between both Vlasov algorithms: (a) time evolution of the mean normalized density and (b) time evolution of the total energy. The full line is related to the time splitting scheme while the dotted line corresponds to the 2D full advection. Exact integration of the Vlasov equation can be achieved only by the full 2D advection algorithm.

the growth of several plasma modes as can be seen in Figs. 2(a) and (b) showing the time evolution of the most unstable plasma modes (modes $3\Delta k$ and $4\Delta k$) on a logarithmic scale. In Fig. 2 no initial perturbation has been introduced in the distribution function: both Vlasov models being noiseless, the longitudinal electric field starts up from the round-off errors (initially of order of 10^{-16}), the density perturbation level was then chosen exactly identical in both models.

Here the full line corresponds to the splitting model whereas the dotted line is related to the 2D advection model: both methods indicates growth rates in good agreement with the expected values predicted by linear theory ($\gamma_{\mathrm{th}}/\omega_{\mathrm{p}} = 0.289$ for plasma mode $k_{\mathrm{e}}c/\omega_{\mathrm{p}} = 3\Delta k = 1.50$ and $\gamma_{\mathrm{th}}/\omega_{\mathrm{p}} = 0.227$ for the corresponding plasma mode $k_{\mathrm{e}}c/\omega_{\mathrm{p}} = 4\Delta k = 2.0$). Here we have solved the dispersion relation given in [8], i.e.,

$$D_+D_- = \frac{\omega_{\mathrm{p}}^2 a_0^2}{\gamma_0^3}\left(\frac{k^2c^2}{D_{\mathrm{p}}} - 1\right)(D_+ + D_-), \tag{62}$$

where D_{p}, $D_\pm$ correspond, respectively, to the dispersion relation of the electron plasma wave and of the electromagnetic waves in the presence of the large amplitude electromagnetic wave. We have

$$D_{\mathrm{p}} = \omega^2 - \frac{\omega_{\mathrm{p}}^2}{\gamma_0}, \tag{63}$$

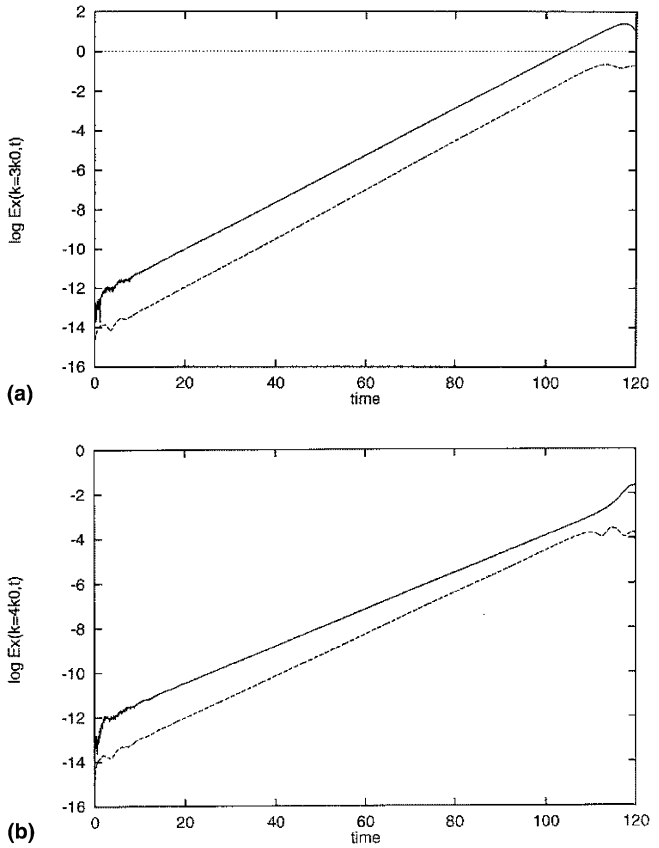

Fig. 2. Time evolution of the most unstable plasma modes ($3\Delta k$ in (a) and $4\Delta k$ in (b)) in the case of the parametric decay of the pump wave in the relativistic regime. A logarithmic scale has been used. Full lines correspond to the TSS whereas dotted lines are related to the semi-Lagrangian model with full 2D advection using B-splines interpolations.

$$D_{\pm} = (\omega \pm \omega_0)^2 - (k \pm k_0)^2 c^2 - \frac{\omega_p^2}{\gamma_0}. \tag{64}$$

The numerical values using TSS for the numerical resolution of the Vlasov equation are $\gamma_{num}/\omega_p \simeq 0.276$ for $k_e c/\omega_p = 1.50$ and $\gamma_{num}/\omega_p \simeq 0.192$ for $k_e c/\omega_p = 2$. A direct integration scheme using 2D advection leads to more precise values of the growth rate of the relativistic modulational instability: $\gamma_{num}/\omega_p \simeq 0.284$ for $k_e c/\omega_p = 1.50$ and $\gamma_{num}/\omega_p \simeq 0.218$ for $k_e c/\omega_p = 2$.

Thus, during the linear stage of the instability (i.e., $t\omega_p \leqslant 100$), although the invariants are well conserved in both codes, the growth rates are in well better agreement for the 2D scheme than for the TSS.

Since the wave generation mechanism is resonant, the wave grows secularly until nonlinear effects cause plasma wave breaking and limit thus the plasma wave growth around $t\omega_p \sim 100$. At that time, the TSS code leads to bad conservation, so that the saturation processes will not be carefully described. There are important differences between Figs. 3 and 4 which can be related to the nonlinear interaction between the trapped electrons and the plasma wave. Clearly the splitting procedure here cannot describe correctly the saturation mechanism of the relativistic modulational instability due to a bad density conservation. The complex electron phase space behavior is shown in Fig. 3 for the TSS model; the corresponding curves obtained with the other method are displayed in Fig. 4. As the plasma wave rises, the formation of phase space vortices is clear in Fig. 4 and, as the plasma wave fields saturates, plasma wave breaking becomes evident at time $t\omega_p = 113$ with the occurring of a strong particle acceleration. The behavior of the electron distribution function is very different in Fig. 3.

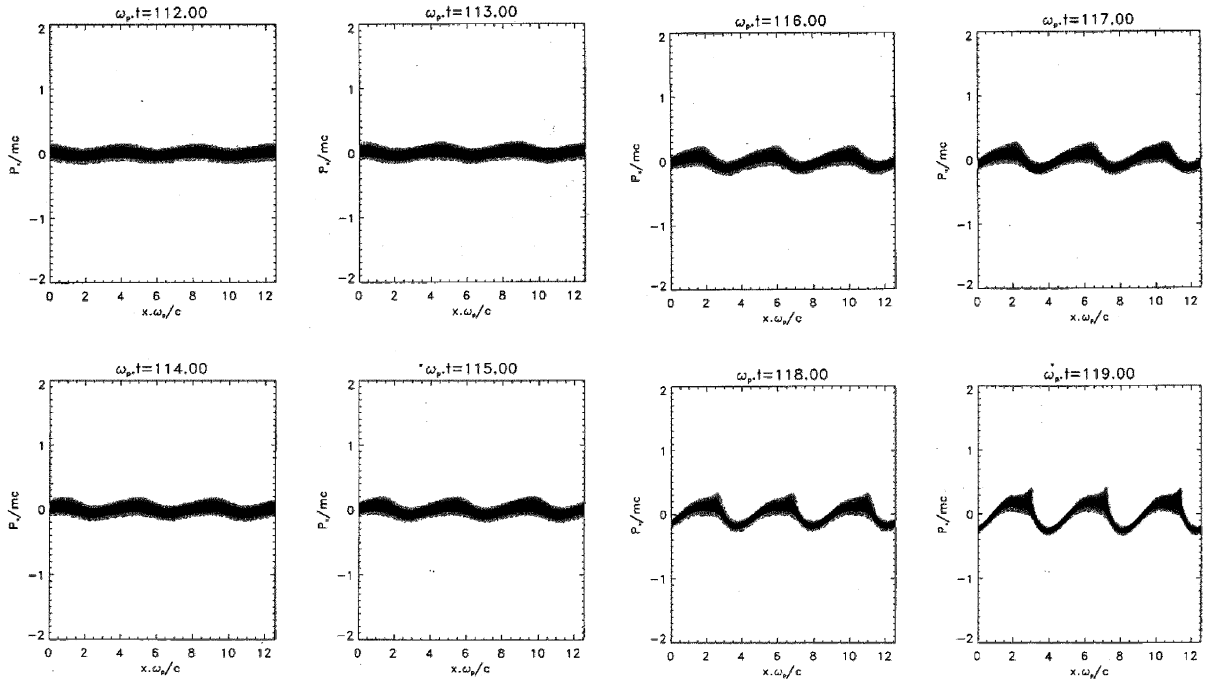

Fig. 3. The $x - p_x$ electron phase space representation afforded by the numerical Vlasov code using TSS in the case of the study of the modulational instability in the relativistic regime. The parameters of the simulation are $n/n_{crit} = 0.55$, $a_0 = 0.75$ and $k_0 c/\omega_p = 1$.

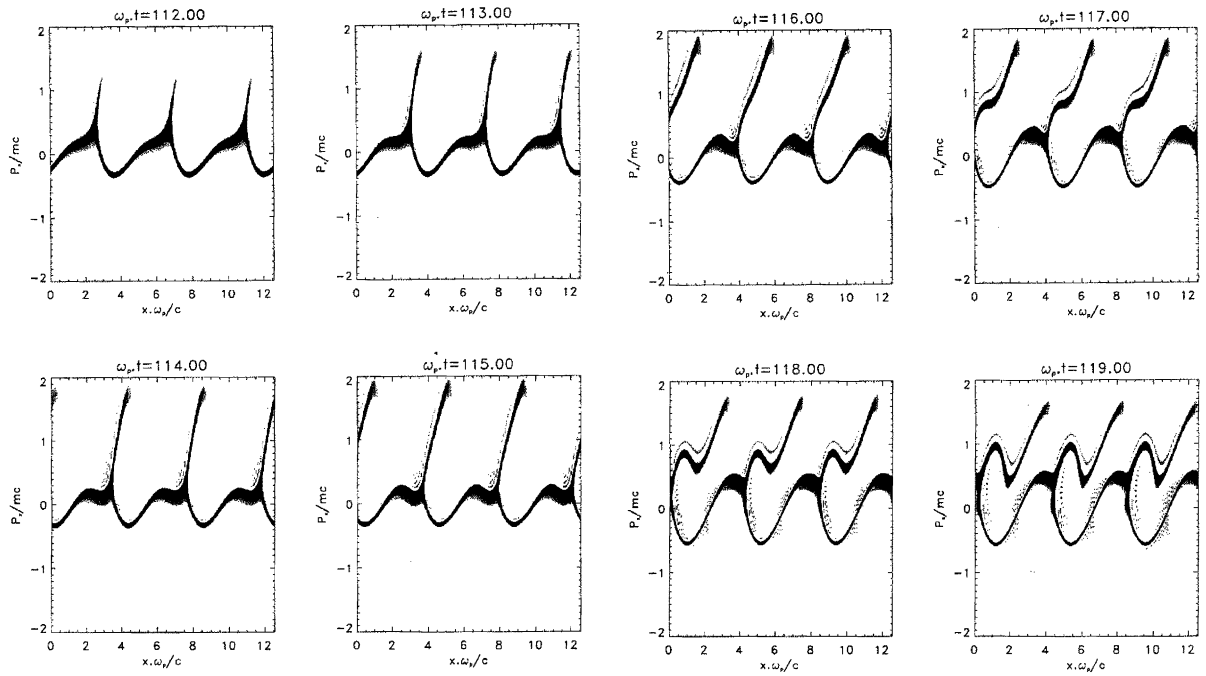

Fig. 4. Corresponding $x - p_x$ electron phase space representation of the distribution function computed through 2D full advection and 2D B-spline interpolations. The comparison with Fig. 3 also makes it clear that TSS cannot be adequate here since it leads to numerical instability after time $t\omega_p \geqslant 120$ at the saturation of the relativistic modulational instability.

4.2. Causal $(x - t)$ Vlasov simulations of the self-induced transparency

Vlasov causal simulations for moderate pump intensities have been already published (see [15–17]) which display phase space features similar to those shown in the periodic cases at the same intensities. The spatial causality of the periodic case is fatally flawed, since when an electromagnetic field reaches a boundary in a periodic code its image simultaneously appears to the other boundary. Also, the growth of a rapid instability is quite different when the pump is incident on the plasma, rather than existing a time zero with no instability developed. In fact, we require a realistic bounded plasma with transparent walls: the electron distribution function is fixed by $f(x = 0, p_x, t) = 0$ and $f(x = L, p_x, t) = f_{\mathrm{Max}}(p_x)$, where f_{Max} is the Maxwellian distribution function. The electromagnetic radiations are allowed to enter the system at the left boundary, when exiting at the other boundary, they do not return and are no longer considered. For right circularly polarized electromagnetic fields, we assume

$$E^+(x = 0, t) = 2E_0 P(t) \cos \omega_0 t; \quad E^-(x = 0, t) = 0, \tag{65}$$

$$F^+(x = 0, t) = 0; \quad F^-(x = 0, t) = -2\varepsilon E_0 P(t) \sin \omega_0 t \tag{66}$$

and for the momentum

$$P_y(x = 0, t) = \frac{eE_0 P(t)}{\omega_0} \sin \omega_0 t, \tag{67}$$

$$P_z(x=0,t)=\frac{eE_0\varepsilon P(t)}{\omega_0}\cos\omega_0 t \tag{68}$$

in which the rise time profile P is given by: $P(t)=\sin^2\pi t/2\tau$ for $t\leqslant\tau$ and $P(t)=1$ for $t\geqslant\tau$ (and $\tau\omega_p=50$). It is well known that a high frequency electromagnetic wave, with frequency less than the electron plasma wave ($\omega_0<\omega_p$) cannot propagate in a plasma. But if the intensity of the pump wave is sufficiently intense, to make electrons relativistic, the cutoff frequency ω_p is then modified due to relativistic mass variation. The condition previously studied in Section 4 corresponds to an underdense plasma. In the following, a laser pulse propagation in the x-direction is normally incident on an inhomogeneous density profile in the case of an overdense plasma. For the simulations presented here, the ions form an immobile background with steep gradient in density and the electron density is $n_0/n_{crit}=1.50$. The irradiation is $I\lambda^2=8.20\times 10^{18}$ W cm^{-2} μm^2, which corresponds to a normalized quiver momentum of $a_0=\sqrt{3}$. The relativistic factor in vacuum is then $\gamma_0=\sqrt{1+a_0^2}=2$ leading to $n_0/\gamma_0 n_{crit}=0.75$. The phase space sampling is identical in both simulations $N_xN_{p_x}=2048\times 384=786\,432$ "particles" or grid points. We use a time step of $\Delta t\omega_p=0.025$. Again we used two algorithms for solving the Vlasov equation. One was the standard TSS algorithm. The other was a full bidimensional advection in order to make comparisons. With the two algorithms we studied the dependence of the results on the accuracy with which the Vlasov equation was integrated.

Fig. 5 display the mean density conservation in time. Solid line corresponds to the 2D advection while the dotted line is related to the numerical integration using time splitting. The onset of numerical noise induced by splitting was clearly evident. As one can see, the dotted line used in Fig. 5 indicates that the mean density strongly varies in time showing an inadequate use of the TSS in that case when relativistic effects are dominant.

The onset of numerical instability occurred at approximately the time $t\omega_p=80$. Fig. 6 shows, at time $t\omega_p=75$, the behavior of the longitudinal electric fields (given in $m\omega_p c/e$ units) in both simulation tests: solid line corresponds to the full 2D advection while the dotted line is obtained in the case of a splitting. The electric field has been determined by solving a centered finite-difference approximation to Ampere's equation with the charge current evaluation at time t_n where the distribution function can be exactly evaluated. Although the longitudinal electric field was computed from the Ampere equation (57), the Poisson equation is used to take into account the boundary conditions which are identical in both models. Starting from the Poisson equation (51), we can evaluate the values of the electric field at the box boundaries after integration over the length of the system, we obtain

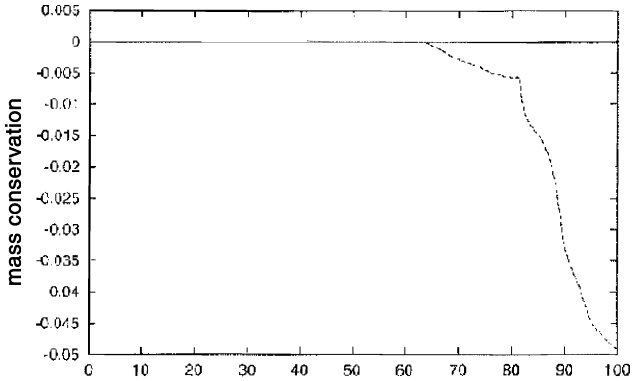

Fig. 5. Display of the mean density conservation versus time. Again solid lines (dotted lines) correspond to the 2D full advection (respectively to TSS). The onset of numerical noise induced by TSS was clearly evident.

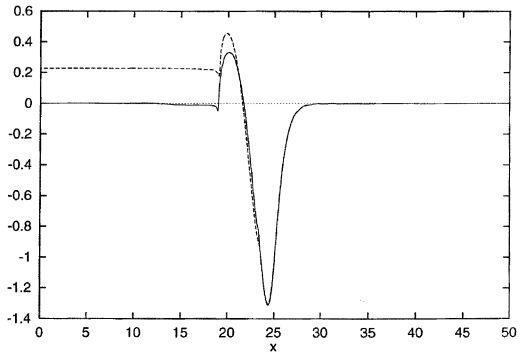

Fig. 6. Behavior of the longitudinal electric field (given in $m\omega_p e/c$ unit) in both simulation tests: solid line corresponds to the 2D exact advection and dotted line to TSS. A strong electric field develops at the left boundary of the plasma system (in dotted line) as the result of a bad mass conservation of the numerical algorithm based on TSS.

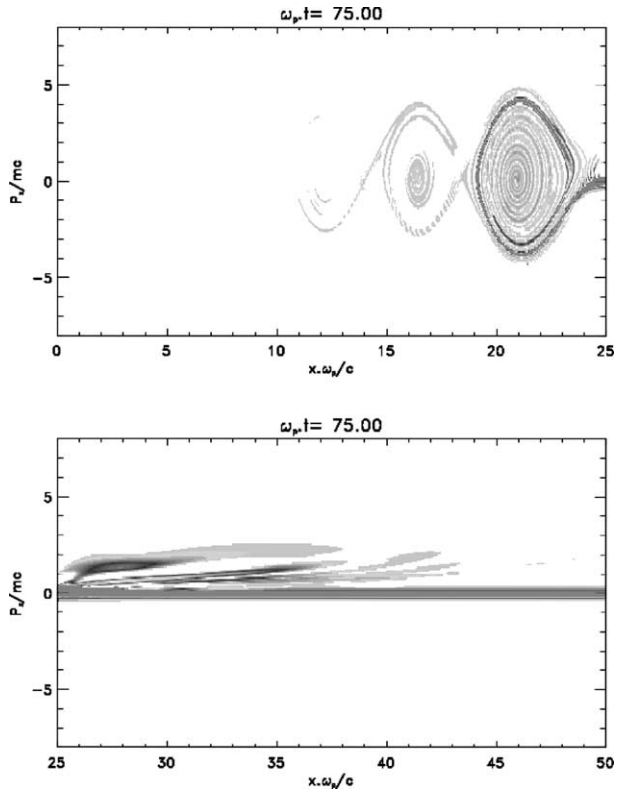

Fig. 7. Phase space representation of the electron distribution function at the beginning of the laser–plasma interaction at time $t\omega_p = 75$. The curve was obtained using the TSS algorithm. The plot has been separated into two parts in x in order to obtain a more precise description of the distribution function.

$$E_x(L) - E_x(0) = \int_0^L \frac{e}{\varepsilon_0}(n_e - n_i)\,dx. \tag{69}$$

Taking $E_x(L) = 0$ (assuming that the electromagnetic field has not reached the right side of the plasma box) we obtain then for the boundary condition of the longitudinal field at $x\omega_p/c = 0$:

$$E_x(0) = -\int_0^L \frac{e}{\varepsilon_0}(n_e - n_i)\,dx. \tag{70}$$

Eq. (70) allows us to take into account the particles which physically leave the system at the leftside of the system (however this particle number remains small in simulation). As mentioned in Section 3.3, in the TSS model the Poisson equation is used at the end of the step A1, after the first shift in the x-direction, while in the second code using the 2D advection, the Ampere equation given by Eq. (57) is first used as a predictor and then the Poisson equation is used at the end of the 2D advection as a corrector (the obtained values are then used in the Ampere equation at the next time step).

As illustrated in Fig. 6, a strong electric field amplitude develops at the left boundary of the system (in dotted line) as the result of the violation of the conditions (16) and (17) which are the necessary conditions for applying the TSS. Note at this step of the numerical simulation, energetic electrons produced by the relativistic instability have not reached the plasma boundaries: the growth of the longitudinal field at the

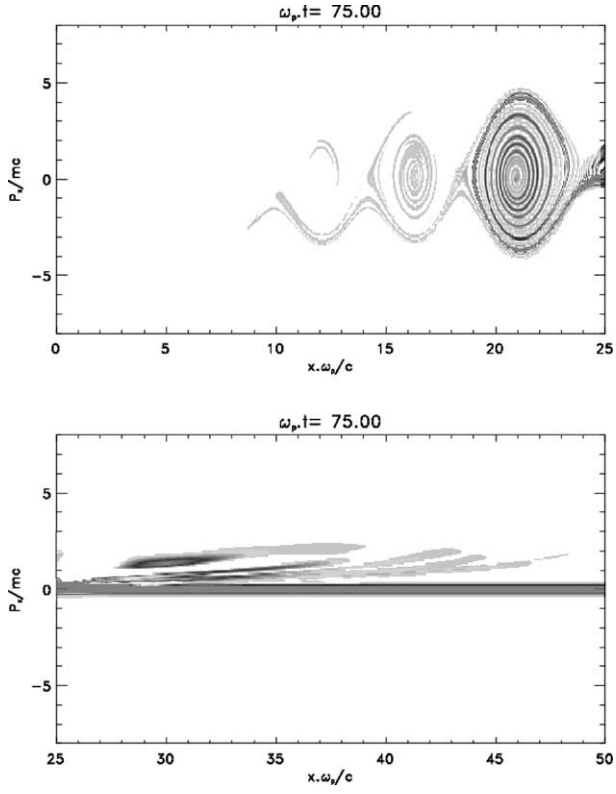

Fig. 8. Corresponding particle distribution function in phase space directly obtained by the 2D full advection in the semi-Lagrangian algorithm. The distribution function was plotted at the same time $t\omega_p = 75$ (see Fig. 7). This algorithm, due to its accuracy allows a very fine resolution in phase space and particularly of the particle dynamics inside the vortex.

left boundary is principally due to the numerical increase of charge density. In the other hand, in the case of the full 2D advection algorithm, the Vlasov equation was integrated more accurately and the electric field was rather correct at the left boundary (plotted in solid line). In both cases numerical simulations show the

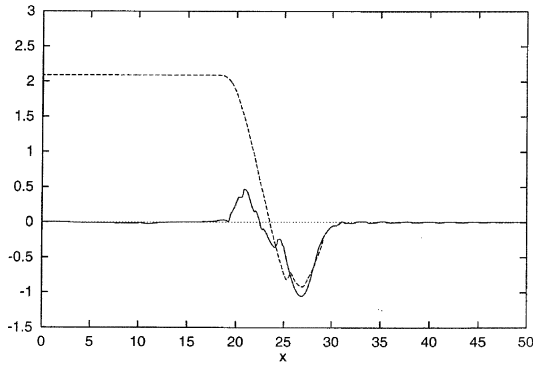

Fig. 9. Display of the the longitudinal electric field versus space at time $t\omega_p = 94$. A comparison between both numerical schemes of the Vlasov equation was carried out: the TSS algorithm gives rise to numerical instability in the case of integration of the relativistic Vlasov equation whereas the full 2D advection algorithm remains stable.

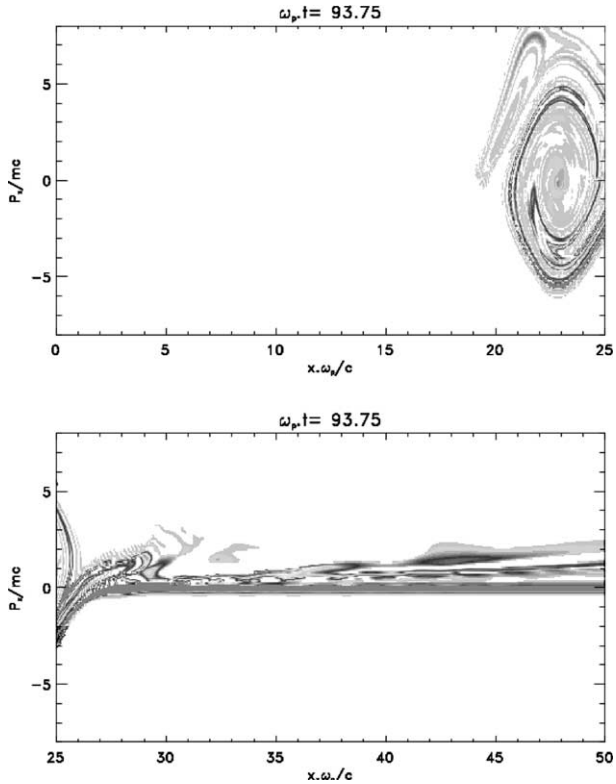

Fig. 10. Display of the electron distribution function in phase space using the TSS algorithm at the same time $t\omega_p = 94$. The comparison with the second method is presented in Fig. 11.

formation of a strong pulse amplitude at the critical surface where the electromagnetic wave is penetrating by induced transparency inside the overdense plasma.

The behavior of the electron distribution function in phase space at the beginning of the electromagnetic pulse penetration is presented in Fig. 7 in the case of the TSS algorithm. The corresponding curve obtained with the full 2D advection is displayed in Fig. 8 at the same time $t\omega_p = 75$. In both figures, the plot has been separated into two parts in x in order to obtain a more precise view of the distribution function in phase space.

As the result of particle trapping, the figures exhibit the formation of a vortex structure with spiral orbits in phase space. The 2D advection algorithm, due to its accuracy allows a very fine resolution in phase space, particularly inside the vortex. The spirals (six in Fig. 8) inside the vortex structure implicitly reflect the history of particles as the wave has built up. Note that an inadequate use of the splitting of the Vlasov equation here do not provide the same fine resolution all over the phase space. Ions being immobile, the non-conservation in the electron density leads to a strong increase of the electric field at the leftside of the plasma system according to Eq. (70), which modifies strongly the trapping structure in phase space. Results of simulation at later time $t\omega_p = 94$ were shown in Figs. 9–11. As stated earlier the time splitting algorithm gives rise to a strong electric field at the left boundary of the simulation box leading to numerical instability. The growth of this numerical instability is clearly evident in graphs of electric field versus space in Fig. 9 (the dotted line corresponds to the splitting scheme). Fig. 10 is a phase space plot from the time splitting scheme while the corresponding plot obtained by the other method is shown in Fig. 11. Because of presence

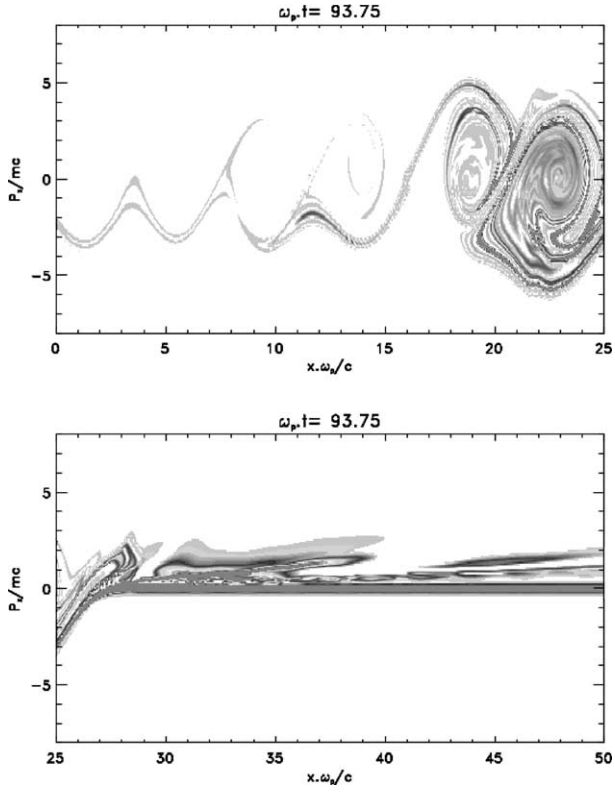

Fig. 11. Display of the corresponding phase space representation of the electron distribution function at time $t\omega_p = 94$ obtained through a semi-Lagrangian scheme using direct 2D advection in $x - p_x$ phase space. Because of the presence of numerical instability induced by TSS (see Fig. 10) the plasma evolution differs strongly.

of the strong numerical field induced by a bad mass conservation at the left boundary of the system, plasma evolution now strongly differs.

5. Conclusion and perspectives

In this paper, we have presented some examples related to the study of the laser–plasma interaction in the relativistic regime which could not be solved accurately using the splitting procedure of the Vlasov equation. It would appear that the direct integration using 2D full advection in this kind of problems is necessary for achieving accurate solutions of the Vlasov–Maxwell system. It is important to point out that the splitting method does not trigger any underlying numerical instability, but it is necessary to use it in such a way that phase space measure be conserved locally at each integration step.

The scheme of time splitting is now commonly used in the community of plasma physics for solving the Vlasov equation in Eulerian model and works very well for electrostatic problems. The use of the TSS algorithm in collisionless plasma simulation has contributed greatly to the present day understanding and application of plasma physics, this technique has nevertheless shortcoming that prohibit application to some important and interesting problems as guiding-centre problem or the treatment of the relativistic Vlasov equation in the 2D phase space. In order to avoid these difficulties it would probably necessary to use 2D (or 3D) full advection schemes that treated features of particles dynamics more accurately.

The science and art of numerical plasma simulation is a powerful tool in plasma physics. However, its applicability would be even greater if practical semi-Lagrangian methods using both 2D full advection and splitting scheme were used in more general problems. It would be the case, for the 2D spatial relativistic and electromagnetic Vlasov model in which space and momentum contribution could be separated using splitting scheme and two 2D full advection used for the **x** and **p** integration. Numerical results would be published in due course.

Acknowledgements

The authors are indebted to the IDRIS center (Institut du Developpement et des Ressources en Informatique Scientifique, Orsay, France) for computer time allocation on the NEC-SX5 computer.

References

[1] C.Z. Cheng, G. Knorr, The integration of the Vlasov equation in configuration space, J. Comput. Phys. 22 (1976) 330.
[2] C.Z. Cheng, The integration of the Vlasov equation for a magnetized plasma, J. Comput. Phys. 24 (1977) 348.
[3] R. Gagné, M. Shoucri, A splitting scheme for the numerical solution of a one-dimensional Vlasov equation, J. Comput. Phys. 24 (1977) 445.
[4] M. Shoucri, Numerical solution of the two-dimensional Vlasov equation, IEEE Trans. Plasma Sci. PS7 (No. 2) (1979) 69.
[5] E. Sonnendrücker, J. Roche, P. Bertrand, A. Ghizzo, The semi-Lagrangian method for the numerical resolution of Vlasov equations, J. Comput. Phys. 149 (1998) 201.
[6] A. Ghizzo, P. Bertrand, M.M. Shoucri, T.W. Johnston, E. Fijalkow, M.R. Feix, A Vlasov code for the numerical simulation of stimulated Raman scattering, J. Comput. Phys. 90 (1990) 431.
[7] A. Ghizzo, P. Bertrand, M.L. Begué, T.W. Johnston, M. Shoucri, A Hilbert–Vlasov code for the study of high-frequency plasma beatwave accelerator, IEEE Trans. Plasma Sci. 24 (1996) 370.
[8] S. Guérin, G. Laval, P. Mora, J.C. Adam, A. Héron, A. Bendid, Modulational and Raman instabilities in the relativistic regime, Phys. Plasmas 2 (7) (1995) 2807.
[9] P. Mora, T.M. Antonsen, Kinetic modeling of intense, short laser pulses propagating in tenuous plasmas, Phys. Plasmas 4 (1) (1997) 217.

[10] M.L. Begué, A. Ghizzo, P. Bertrand, Two dimensional Vlasov simulation of Raman scattering and plasma beatwave acceleration on parallel computer, J. Comput. Phys. 151 (1999) 458.
[11] M.L. Begué, A. Ghizzo, P. Bertrand, E. Sonnendrücker, O. Coulaud, Two dimensional semi-Lagrangian Vlasov simulation of the laser–plasma interaction in the relativistic regime, J. Plasma Phys. 62 (part 4) (1999) 367.
[12] A. Staniforth, J. Côté, Semi-Lagrangian integration schemes for atmospheric models, A review, Mon. Weather Rev. 119 (1991) 2206.
[13] R. Bermejo, Analysis of an algorithm for the Galerkin-characteristic method, Numer. Math. 60 (1991).
[14] G.I. Marchuk, Methods of Numerical Mathematics, Springer-Verlag, New York, 1982.
[15] P. Bertrand, A. Ghizzo, T.W. Johnston, M. Shoucri, E. Fijalkow, M.R. Feix, A nonperiodic Euler–Vlasov code for the numerical simulation of laser–plasma beatwave acceleration and Raman scattering, Phys. Fluids B 2 (5) (1990) 1028.
[16] P. Bertrand, A. Ghizzo, S.J. Karttunen, T.J.H. Pättikangas, R.R.E. Salomaa, M. Shoucri, Two-stage electron acceleration by simultaneous stimulated Raman backward and forward scattering, Phys. Plasmas 2 (8) (1995) 3115.
[17] P. Bertrand, A. Ghizzo, S.J. Karttunen, T.J.H. Pättikangas, R.R.E. Salomaa, M. Shoucri, Simulations of wave-particle interactions in stimulated Raman forward scattering in a magnetized plasma, Phys. Fluids B 4 (11) (1992) 3590.